Orientation and Conformation of a Lipase at an Interface Studied by Molecular Dynamics Simulations

Morten Ø. Jensen,* Torben R. Jensen,[†] Kristian Kjaer,[‡] Thomas Bjørnholm,[§] Ole G. Mouritsen,[¶] and Günther H. Peters*

*Center for Biomembrane Physics (MEMPHYS), Department of Chemistry, Technical University of Denmark, DK-2800 Lyngby, Denmark; [†]Department of Chemistry, University of Aarhus, DK-8000 Århus C, Denmark; [‡]Condensed Matter Physics and Chemistry Department, Risø National Laboratory, DK-4000 Roskilde, Denmark; [§]Nano-Science Center, Chemistry Department, University of Copenhagen, Universitetsparken 5, DK-2100 Copenhagen Ø, Denmark; and [¶]Center for Biomembrane Physics (MEMPHYS), Physics Department, University of Southern Denmark, DK-5230 Odense M, Denmark

ABSTRACT   Electron density profiles calculated from molecular dynamics trajectories are used to deduce the orientation and conformation of *Thermomyces lanuginosa* lipase and a mutant adsorbed at an air-water interface. It is demonstrated that the profiles display distinct fine structures, which uniquely characterize enzyme orientation and conformation. The density profiles are, on the nanosecond timescale, determined by the average enzyme conformation. We outline a computational scheme that from a single molecular dynamics trajectory allows for extraction of electron density profiles referring to different orientations of the lipase relative to an implicit interface. Profiles calculated for the inactive and active conformations of the lipase are compared with experimental electron density profiles measured by x-ray reflectivity for the lipase adsorbed at an air-water interface. The experimental profiles contain less fine structural information than the calculated profiles because the resolution of the experiment is limited by the intrinsic surface roughness of water. Least squares fits of the calculated profiles to the experimental profiles provide areas per adsorbed enzyme and suggest that *Thermomyces lanuginosa* lipase adsorbs to the air-water interface in a semiopen conformation with the lid oriented away from the interface.

INTRODUCTION

Lipases (triacylglycerol hydrolases, EC 3.1.1.3) are enzymes, catalyzing both the hydrolysis and the synthesis of esters formed from glycerol and long-chain fatty acids. In addition to triglycerides, lipases are also able to catalyze hydrolysis and synthesis of a wide range of soluble and insoluble organic compounds making them potential catalysts for a wide variety of applications in chemical industries, biomedical sciences, and food technology.

The activation mechanism of these lipases has partly been revealed by their crystal structures (Derewenda et al., 1994; Brzozowski et al., 1991). The first lipase, resolved in the open (active) and inactive (closed) conformation, was the *Rhizomucor miehei* lipase (Brady et al., 1990; Derewenda et al., 1992). The crystal structures of this lipase indicate that the conformational change during activation is a rigid body hinge-type motion of a single helix. This type of motion is more complex for other lipases, involving hinge-type motions of multiple helices (Derewenda et al., 1994).

In the present study, we focus on the *Thermomyces lanuginosa* lipase (Tll) formerly named *Humicola lanugi-*

nosa, crystallized in the open and closed conformation (Derewenda et al., 1994, 1992; Brzozowski et al., 1992, 2000). Tll shares, with other lipases, the characteristic structural α/β hydrolase fold (Grochulski et al., 1993) and possesses a trypsin-like triad consisting of a Ser/His/acidic residue active site region and a neighboring oxyanion hole. The Ser residue in the sequence G-X-S-X-G (X denotes any residue) forms the nucleophilic center, and His acts as a general acid/base. The acidic residue in the triad mediates the protonation of His during catalysis. The oxyanion hole stabilizes the incipient carbonyl of the ester group during turnover. As other lipases, Tll requires a lipid-water interface to exert full catalytic activity; i.e., the substrate concentration must exceed the critical micelle concentration (Panaiotov et al., 1997). The lipid interface triggers a conformational change in the enzyme that, as observed for the related *R. miehei* lipase, involves displacement of an α-helical lid shielding the active site in aqueous solution. This displacement is essential for providing access of the substrate to the active site and, at the same time, exposes a hydrophobic part of the lid toward the lipid, thereby mediating binding of the lipase to the interface (Derewenda et al., 1994). Interactions between the lipid interface and hydrophobic residues of the lid contribute to the stabilization of the open conformation and the conformational rearrangements of the enzyme at the lipid interface correlate intimately with the phenomenon of interfacial activation (Derewenda et al., 1994).

A central issue in relating the conformational changes of lipases to their biological function is to understand to what extent these enzymes bind to, react with, or become catalytically activated by lipid-water interfaces (Rubingh,

---

1996). The presence of a structured lipid interface with subtle physical properties adds another complexity to the problem of explaining the response of the enzyme when in contact with the interface. Different mechanisms of interfacial activation, which can be classified in two extremes, have been proposed (Thuren, 1988; Derewenda et al., 1994; Peters et al., 1995). One is based on a substrate-mediated mechanism (Thuren, 1988), suggesting that changes in the physical properties of the lipid substrate such as hydration, fluidity, curvature, charge, and composition trigger the activation, whereas the other proposed mechanism involves conformational changes in the enzyme upon adsorption to the lipid interface (Derewenda et al., 1994). It should be noted that these schemes are not mutually exclusive (Peters et al., 1995), and refined kinetic models involving both of them have been suggested (Brzozowski et al., 1991; van Tilbeurgh et al., 1993; Verger et al., 1984; Ransac et al., 1990, 1991). These include a two-step mechanism initialized by adsorption of the enzyme at the interface followed by formation of an enzyme/substrate complex (Brzozowski et al., 1991; van Tilbeurgh et al., 1993; Verger et al., 1984).

A detailed insight into the mechanism of lipolytic hydrolysis requires that the binding of the lipase to the lipid interface, its subsequent/simultaneous activation, and ultimately, the catalytic reaction all can be investigated independently with respect to the physical properties of the lipid interface. One approach is to study the adsorption of lipases to different lipids using lipid monolayers (Panaiotov et al., 1997) or liposomes (Cajal et al., 2000; Jutila et al., 2000; Peters et al., 1998). The most detailed insight into interfacial binding of lipases at the molecular level has, however, been obtained by ESR experiments (Ball et al., 1999). Frequently used techniques such as Langmuir monolayer methods (Verger and de Haas, 1973) and fluorescence spectroscopy (Kinnunen et al., 1993; Millar, 1996) have yet to provide such information, although nanosecond dynamics of the lid movement have been monitored by time-resolved fluorescence spectroscopy (Jutila et al., 2000). Nevertheless, information about the orientation and conformation of the lipase at the interface as well as complete description of the triggering mechanism associated with interfacial activation are still lacking.

Surface sensitive synchrotron x-ray scattering has proven useful for investigation of biological systems assembled as thin films at the air-water interface (Alonso, et al., 2001; Rapaport et al., 2000; Jensen et al., 2001). To gain structural insight into the orientation and conformation of Tll at a hydrophobic-hydrophilic interface, we have measured the x-ray reflectivity of lipases adsorbed at an air-water interface. This interface is the simplest representation of a hydrophobic-hydrophilic interface and is a first step towards studying Tll at more complex interfaces (lipid-water). Although electron density profiles can be extracted from the reflectivity curve, the profiles are not uniquely determined due to the crystallographic phase problem (Jensen and

Kjaer, 2001). Furthermore, the interpretation of the reflectivity data in terms of enzyme conformation and orientation is not trivial. In the present work, we demonstrate that molecular dynamics (MD) simulations can be used in interpreting the experimental electron density profiles in terms of enzyme conformation, orientation, and surface concentration.

Several MD simulations of triacylglyceride lipases have been reported (Peters et al., 1995, 1996a, 1996b, 1998; Brzozowski, 2000), but to our knowledge, no study addresses the question of enzyme orientation and conformation at an interface. Here, we outline a computational scheme by which one can extract electron density profiles from an MD trajectory that refers to an average enzyme orientation relative to an implicit interface. The computed profiles can be compared with profiles extracted from our x-ray reflectivity measurements to provide the most probable orientation and conformation of Tll at the interface.

MATERIALS AND METHODS

In the following we briefly describe the MD simulations and the x-ray reflectivity experiments. We then outline the method for extraction of multiple electron density profiles from a single trajectory along with the procedure for comparing calculated and experimental electron density profiles.

Modeling and simulation

We carried out MD simulations on both the closed and open conformations of Tll in cubic simulation boxes with explicit water. These two conformations are the two extremes of possible Tll conformations. We carried out simulations without an explicit air-water interface, because the reflectivity data indicate that the major part of each adsorbed lipase molecule is embedded in the water phase. Furthermore, the part of the experimental electron density profile providing structural information refers manifestly to the water phase (see Results and Discussion). For purposes of analysis, we incorporated an implicit interface (see below).

Starting coordinates for the open conformation were obtained from the Protein Data Bank (Bernstein et al., 1977), entry code 1TIC. The coordinates for the closed conformation were kindly provided by Prof. M. Brzozowski. These structures are resolved to 2.5 Å (closed) and 2.6 Å (open). Enzymes of either conformation were initially placed in simulation boxes of volume $59 \times 59 \times 59$ Å^3 with the active site lid pointing along the normal to the interface, i.e., in the direction of n_z (Fig. 1).

To saturate the enzyme interior with water, water molecules were initially inserted into sufficiently large protein cavities in the open conformation of Tll using the program QUANTA97 (MSI, 1997). Insertion was possible in a few (14) hydrophilic pockets. No additional water molecules were inserted inside the closed conformation. The enzymes were solvated using an equilibrated configuration of ~5000 SPC water molecules. The net negative charges of the enzymes were in both systems neutralized by replacing seven water molecules by Na$^+$ ions at positions of lowest Coulomb potential. The total system sizes were ~20,000 atoms.

The program Gromacs (Berendsen and van der Spoel, 1995) was used with the Gromos 87 force field (van Gunsteren and Berendsen, 1987) for the simulations. The simulations were conducted in the *NPT* ensemble at 300 K (temperature-coupling constant 0.1 ps) with the Berendsen pressure-coupling scheme (pressure-coupling constant 1.0 ps) (Berendsen et al., 1984). A 2-fs time-step was used throughout, and van der Waals and Coulomb interactions were computed within cutoffs of 10 and 14 Å,
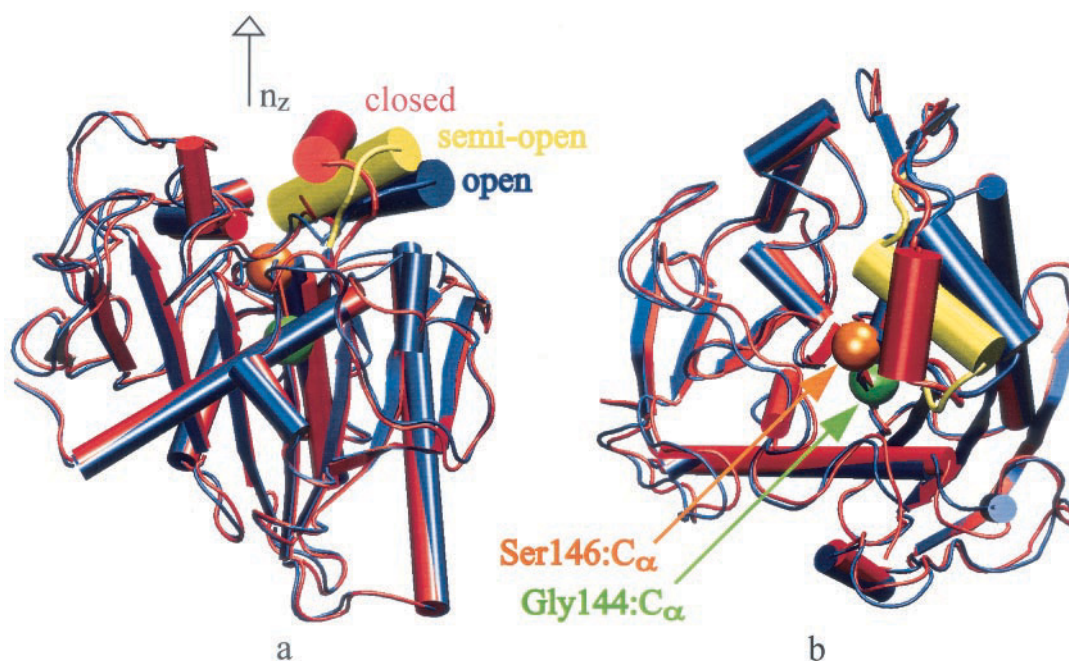
FIGURE 1   Superposition of open (*blue*) and closed (*red*) conformation of Tll: (*a*) active site lid aligned along the outgoing interfacial normal n_z and (*b*) view towards active site. In the experiment $z = 0$ is defined as the location of the interface, here coinciding with the origin of n_z. RMSD between the C_α carbons of the x-ray structures is 1.6 Å. The lid residues 83 to 96 of the semiopen conformation taken after 10 ns of simulation are shown in yellow. The C_α atoms of residues Gly-144 and Ser-146, which are shown for the open conformation only, are rendered as van der Waals spheres in green and ochre, respectively. During the transition from the closed to the open conformation an additional turn in the α-helical lid is formed involving residues 91 to 94. A similar mechanism has been observed for *Candida rugosa* (Grochulski et al., 1993).

respectively. Periodic boundary conditions were imposed in all directions. Initially, both systems were minimized followed by 10 ps of dynamics where all heavy atoms were harmonically restrained to their initial positions. Subsequently, the restraints were removed, and the simulations were conducted for 10 and 12 ns for the open and closed conformation, respectively.

Synchrotron x-ray scattering

Surface-sensitive synchrotron x-ray scattering of lipase monolayers assembled at the air-water interface was performed at the undulator beamline BW1 at the synchrotron radiation facility HASYLAB (Hamburg, Germany), using a liquid surface diffractometer developed at Risø National Laboratory, Denmark (Als-Nielsen et al., 1994; Weissbuch et al., 1997). The sample cell is a Teflon-made Langmuir film balance placed in a gas-tight container with windows transparent to the x-rays. A glass plate is placed in the trough under the x-ray footprint area to reduce the subphase depth to ~0.3 mm, thereby suppressing mechanically excited long-wavelength waves on the liquid surface (Braslau et al., 1985). The x-ray beam illuminates an area of $\sim 2 \times 50$ mm^2 equivalent to $\sim 10^{13}$ molecules of Tll. The microbial lipase Tll was provided by Novozymes, Inc. (Bagsvaerd, Denmark). Tll is a monomer of 269 amino acids (Fig. 1) with a molecular weight of 2.947×10^4 g/mol. Tll was dissolved in water giving transparent solutions of ~1.1 mg/mL, spread on a MilliQ purified subphase of water ($T = 293$ K) and compressed to a surface pressure, $\pi = 15$ mN/m. An inactive mutant with Ser-146 mutated to Ala (denoted S146A) was also investigated.

To obtain information about the vertical (laterally averaged) structure of an interface, a purely vertical scattering vector is required (Jensen and Kjaer, 2001). This can be achieved using specular x-ray reflectivity with equal angles between the surface and the incident and reflected x-rays; $\alpha_i = \alpha_f \equiv \alpha$. The scattering vector q_z then becomes

$$q_z = 2k \sin(\alpha) = 4\pi\lambda^{-1} \sin(\alpha) \qquad (1)$$

The so-called "master formula for reflectivity" relates the measured reflectivity, $R(q_z)$, (kinematically) to the electron density profile along the normal n_z (Als-Nielsen et al., 1994; Als-Nielsen and McMorrow, 2001; Kjaer, 1994)

$$R(q_z) = R_F(q_z) \left| \frac{1}{\rho_\infty} \int \frac{d\rho(z)}{dz} \exp(iq_z z) dz \right|^2 \qquad (2)$$

The Fresnel reflectivity, $R_F(q_z)$, is calculated from standard optics (Born and Wolf, 1984) for a perfectly sharp interface between air and a pure subphase of average electron density ρ_∞. The root-mean-square roughness, σ, for a pure water surface caused by thermally excited microscopic capillary waves is $\simeq 3$ Å (Braslau et al., 1985).

The master formula, Eq. 2, gives raise to the phase problem of x-ray crystallography, because the ratio $R(q_z)/R_F(q_z)$ equals the absolute square of the Fourier transform of the normalized gradient of the electron density across the interface. The measured (normalized) reflectivity, $R(q_z)/R_F(q_z)$, can be inverted to yield the laterally averaged electron density, $\rho(z)$; i.e., the density as a function of the vertical z coordinate. However, the phase problem can in some cases give raise to more than one solution for $\rho(z)$.

In the following we denote the experimental profiles obtained from x-ray reflectivity measurements $\rho_e(z)$, and likewise, the electron density profiles calculated from MD, $\rho_c(z)$. $\rho_e(z)$ and $\rho_c(z)$ are further classified by superscripts used to specify whenever the density refers specifically to wild-type (wt) Tll or S146A in the experiment, or to the open or closed conformation of wt Tll in the simulations.
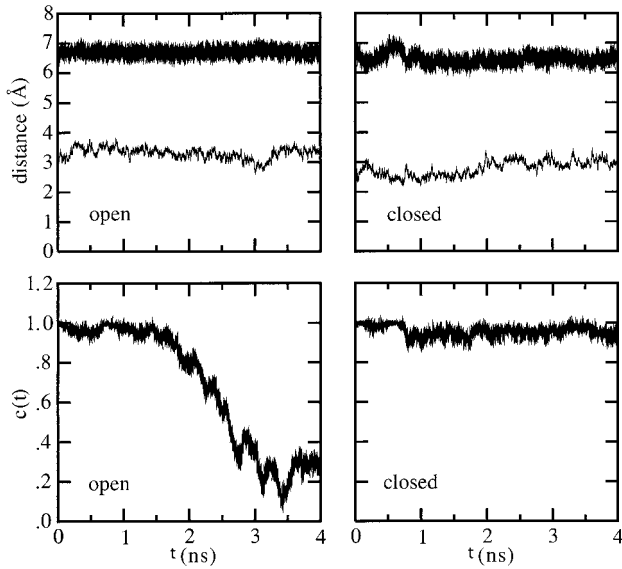
FIGURE 2 (*Upper panels*) Distances $|r_{\text{COM}} - r_{\text{Gly144:C}_\alpha}|$ (*thin*) and $|r_{\text{Gly144:C}_\alpha} - r_{\text{Ser146:C}_\alpha}|$ (*bold*) for the two conformations of Tll as a function of time. (*Lower panels*) Autocorrelation function

$$c(t) = \left[\frac{|r_{\text{Gly144:C}_\alpha} - r_{\text{Ser146:C}_\alpha}|(t = 0) \times |r_{\text{Gly144:C}_\alpha} - r_{\text{Ser146:C}_\alpha}|(t)}{|r_{\text{Gly144:C}_\alpha} - r_{\text{Ser146:C}_\alpha}|(t = 0) \times |r_{\text{Gly144:C}_\alpha} - r_{\text{Ser146:C}_\alpha}|(t = 0)} \right]$$ for

the interfacial alignment vector as a function of time. Gly-144 is located in the hydrophobic core of Tll close to the center of mass (COM) and Ser-146 is the active site residue (Fig. 1). As evident from the upper panels, both of these sites are located at positions generally undergoing minor fluctuations. Therefore, the unit vector $(\hat{r}(t)_{\text{Ser146:C}_\alpha} - \hat{r}(t)_{\text{Gly144:C}_\alpha})$ was used in the alignment procedure (see text for details). The need for the alignment is evident from $c(t)$. In particular the open conformation is seen to rotate significantly during the simulation.

The electron density profile

To interpret $\rho_e(z)$ in terms of enzyme orientation and conformation, we will compare $\rho_c(z)$ obtained for both Tll conformations in different orientations directly with $\rho_e(z)$. However, to accomplish this, two issues must be resolved. The first relates to the discrete nature of the charge representation in the MD force field. The second relates to the computation of $\rho_c(z)$ in a way that uniquely characterizes the enzyme orientation relative to an (implicit) interface.

The discrete charge representation implies that only an inherently discontinuous $\rho_c(z)$ can be extracted from the MD trajectory. The atomic partial electronic charge ($q_{\bar{e}}$) may be Gaussian distributed with a root-mean-square σ using Gaussian convolution, which transforms $q_{\bar{e}}$ of the nth atom at position z_n into a Gaussian. For the N-particle system we obtain the continuous electron density profile as

$$\rho_c(z) = \left\langle \sum_{n=1}^{N} \frac{q_{\bar{e}}}{\sigma_n \sqrt{2\pi}} \exp\left(-\frac{1}{2}\left[\frac{z - z_n}{\sigma_n} \right]^2 \right) \right\rangle \quad q_{\bar{e}} = \bar{e}_n - q_n$$

(3)

in which $\langle \cdot \rangle$ denotes a time average. A universal smearing factor ($\sigma_n = \sigma$) applied for all n atoms is the only physical parameter to be specified in Eq. 3. The maximal value for σ used here is 3 Å, which fully takes into account the roughness of the experimental water surface (Braslau et al., 1985; Jensen and Kjaer, 2001). Assignment of individual σ for different

atoms is superfluous, because $\sigma = 3.0$ Å suppresses the different individual Gaussians.

The second issue arises due to translational and rotational motion of the enzyme (Fig. 2). After the completion of the simulations and prior to the calculations of $\rho_c(z)$, we aligned the unit vector $(\hat{r}(t)_{\text{Ser146:C}_\alpha} - \hat{r}(t)_{\text{Gly144:C}_\alpha})$ (Fig. 1) so it coincides with the surface normal, n_z, thereby leading to a well-defined enzyme orientation. From the aligned enzyme coordinates we generated additional coordinate sets by consecutive rotations that allows for calculation of multiple orientation-specific forms (relative to n_z) of $\rho_c(z)$. Only Tll and the nearest neighboring water molecules located within a radial cutoff of half of the shortest box-length, $r_{\text{cut}}(t)$ (centered on Gly-144:C$_\alpha$), were aligned. Because the simulations were performed at a constant ambient pressure, $r_{\text{cut}}(t)$ is time dependent but sufficiently large to capture the whole enzyme. The alignment was accomplished by requiring that the aligning matrix $R(\phi(t), \theta(t), \psi(t))$ at all t fulfills

$$R(\phi(t), \theta(t), \psi(t)) \times (\hat{r}(t)_{\text{Ser146:C}\alpha} - \hat{r}(t)_{\text{Gly144:C}\alpha})$$

$$= \hat{n}_z(t) \equiv n_z \quad (4)$$

in which $(\phi(t), \theta(t), \psi(t))$ are the Euler angles defining the matrix at t. The rotation aligning the enzyme and the nearby water molecules (altogether N' of the N atoms in total) provides the aligned coordinates $\{r_i'(t)\}_{i=1}^{N'=N'}$. These coordinates are subject to the rotation $R'(\phi', \theta', \psi') \times r_i'(t) = r_i''(t)$ using $\pi/6$ intervals between consecutive (ϕ', θ', ψ'). We calculate the orientation-specific forms of $\rho_c(z)$ from the resulting coordinates $\{r_i''(t)\}_{i=1}^{N'=N'}$. The values $\phi' = 0$, $\theta' = \{m/\pi6\}_{m=1}^{6}$ and $\psi' = \{n/\pi6\}_{n=1}^{11}$ are used in $R'(\phi', \theta', \psi')$. $\rho_c(z)$ is invariant to rotations about the z axis (involving ϕ') and due to symmetry, $\rho_c(z, \phi', \theta', \psi')$ and $\rho_c(z, \phi', -\theta', \psi')$ are identical as are $\rho_c(z, \phi', 0, \psi')$ and $\rho_c(-z, \phi', \pi, \psi')$. All remaining $\rho_c(z)$ are distinct and these we fit to $\rho_e(z)$ to deduce the most probable interfacial orientation and conformation of wt Tll and S146A.

By applying the spherical cutoff $r_{\text{cut}}(t)$ we ignore more distant water molecules in the rotations above, implying that the total amount of water in the simulation box with volume V_1 is not conserved. To correct for this, water with density $\rho_e^{\text{H}_2\text{O}}$, calculated as an average over the outermost water in the box, are added to fill the volume difference $V_1 - V_2$ (V_2 is the sphere volume being determined by $r_{\text{cut}}(t)$). From the electron density profile in the sphere of the time-averaged volume V_2 and from $\rho_e^{\text{H}_2\text{O}}$, the time-averaged orientation specific form of $\rho_c(z)$ in the cubic box of volume V_1 is therefore obtained as

$$\rho_c^{V_1}(z) = N_{\bar{e}}^{\text{total}}/V_1 = [N_{\bar{e}}^{\text{Tll}}(z)/V_2(z)]f(z)$$

$$+ [N_{\bar{e}}^{\text{H}_2\text{O}}(z)/V_2(z)]f(z) + \rho_c^{\text{H}_2\text{O}}[1 - f(z)]$$

$$= \rho_c^{\text{Tll},V_2}(z)f(z) + \rho_c^{\text{H}_2\text{O},V_2}(z)f(z) + \rho_c^{\text{H}_2\text{O}}[1 - f(z)]$$

(5)

$f(z)$ is the ratio between the sphere and square slab volumes

$$f(z) = \frac{\Delta[V_2(z)]}{\Delta[V_1(z)]} = \frac{(\pi/6)dz(6r_{\text{cut}}^2 - 3(z_{\text{low}}^2 + z_{\text{up}}^2) + dz^2)}{L_x L_y dz}$$

(6)

ensuring normalization of $\rho_c(z)$ with the square box volume $V_1 = L_x \times L_y \times L_z$ (omitting time dependencies for clarity). In Eq. 5, $N_{\bar{e}}^{\text{Tll}}$ and $N_{\bar{e}}^{\text{H}_2\text{O}}$ are the number of electrons in Tll and in the water, which is part of the sphere. In Eq. 6, z_{low} and z_{up} are the lower and upper values of z, respectively, defining the slice of the sphere of width dz. Finally, by applying periodic boundary conditions we ensure charge conservation during the convolution of $\rho_c(z)$ and that the water density approaches $\rho_e^{\text{H}_2\text{O}} = 0.333$ Å^{-3} at the box boundaries.
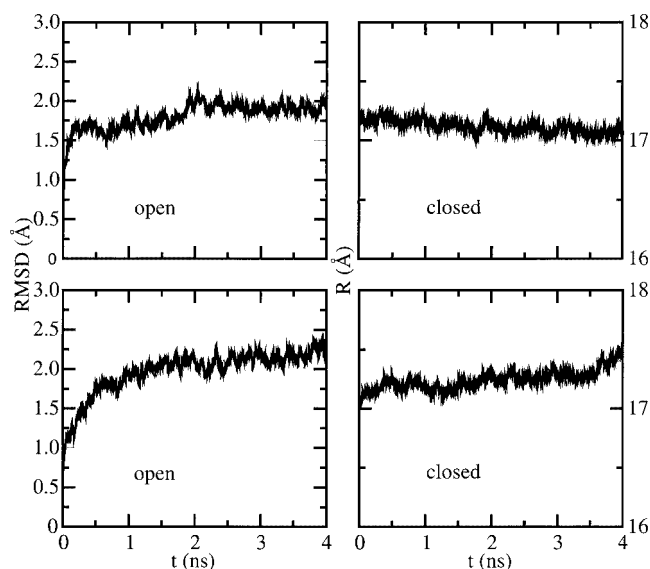
FIGURE 3 RMSD of backbone atoms calculated along the trajectories with respect to the two initial (x-ray) structures for the open and closed conformation of Tll (*left panels*) and total radius, *R*, of gyration (*right panels*).

Least squares fitting

Eqs. 5 and 6 are also used in the least squares fit. $V_1(z) = V_1$ then refers to the experimental volume perpendicular to n_z and $V_2(z) = V_2$ refers to the simulation box volume. We applied $\rho_c^{H_2O}$ and $f = f(z)$ as two fitting parameters. Using $\rho_c^{H_2O}$ (= 0.325 Å^{-3}) as a parameter permits correction for an offset between $\rho_c^{H_2O}$ and $\rho_e^{H_2O}$ (amounting to 2%). Setting $L_2(z) \simeq L_1(z)$ ($= L_c(z) \simeq L_e(z)$) we find $f = A_c/A_e$ and note that the experimental (lateral) area per molecule, A_e, is independent of z. A_e can then be deduced

from linear variation of the calculated lateral box area. Keeping L_z constant, we have $A_e = A_c/f = (L_x \times L_y)/f$. Consequently, we renormalize $\rho_c(z)$ through iterative variation of f while approaching the experimental area per molecule, i.e., the surface concentration. We varied f using intervals of 0.1. Because the interface only appears implicit in the simulations, the origin for $\rho_c(z)$ along the z axis (equivalent to the position of the interface, z_0, in the experiment; Fig. 1) is arbitrarily defined. To translate $\rho_c(z)$ discretely along the z axis with intervals of 0.01 Å, a parameter, Δz, was introduced.

RESULTS AND DISCUSSION

In the following we present and discuss the calculated electron density profiles, $\rho_c(z)$ followed by a comparison of these with the experimental data, $\rho_e(z)$ derived from x-ray reflectivity. Equilibration of the simulations was monitored by thermodynamic and geometric quantities. Radius of gyration and the root mean square displacement (RMSD) of the protein backbone atoms are shown in Fig. 3. RMSD stabilizes at 2 Å after 1 to 2 ns. The radius of gyration is constant over the full time scale. Together with the RMSDs, this indicates that both conformations are stable in the simulations.

Properties of calculated electron density profiles

Raw and convoluted $\rho_c(z)$ are shown in Fig. 4, in which σ values of 0.5, 1.0, 2.0, and 3.0 Å are used to demonstrate the dependence of the fine structure in the electron density profile on this parameter. The intrinsic noise in $\rho_c(z)$ is efficiently removed by the convolution. At the 3-Å level, however, where σ fully includes the effect of surface roughness (Braslau et al., 1985), the fine structure almost vanishes. The $\rho_c(z)$ shown are calculated for both the open and
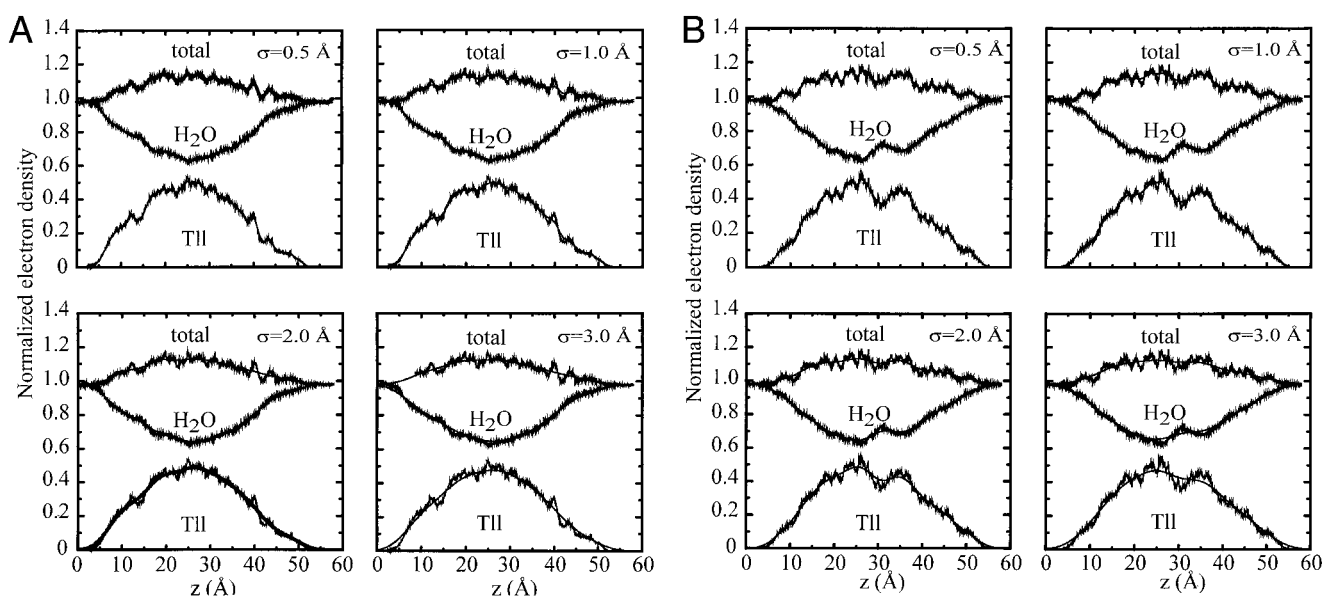

FIGURE 4 Orientation-specific electron density profiles of Tll shown in the (0, 0, 0) orientation: (*A*) closed conformation and (*B*) open conformation. The total profiles are decomposed into contributions from Tll and from water. Raw (noisy) electron density profiles ($\sigma = 0$ Å) appear in all panels and are compared with smeared profiles using various values of σ (respective σ-values are indicated at the top right of each panel). The profiles were averaged over 3 ns.
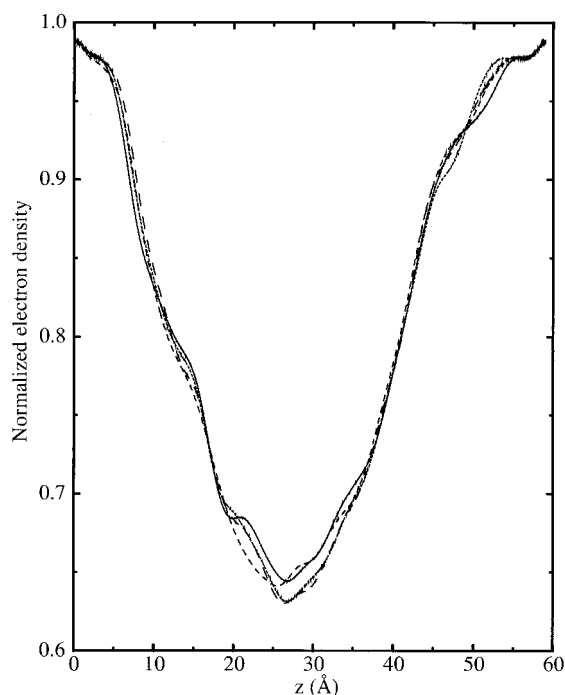
FIGURE 5 Equilibration of the water electron density. The profiles are shown for $\sigma = 1.0$ Å and are averages over 0 to 1 ns (*dashed line*), over 1 to 2 ns (*long dashed line*), over 2 to 3 ns (*dash-dotted*) line, and over 3 to 4 ns (*solid line*). A density of one corresponds to the electron density of bulk water at 300 K (0.333 Å^{-3}).

the closed conformation of Tll in the orientation (0, 0, 0). In this orientation the active site lid points towards the direction of decreasing z; i.e., towards the interface (Fig. 1).

Equilibration of the water density profile is displayed in Fig. 5 at various time instants. The value of $\rho_c^{H_2O}$ that will be added as background density in Eq. 5 to obtain the total $\rho_c(z)$ can be recognized at the box boundaries. This value is consistently found to be below one implying that $\rho_e^{H_2O}$ is not completely recovered in the simulations. The discrepancy is within 2%. The determination of $\rho_c^{H_2O}$ is subject to large fluctuations close to the boundaries due to the small slab volumes of the (spherical) slices at the box boundaries (slab width < 0.03 Å) used in Eqs. 5 and 6. This effect vanishes as σ approaches 3 Å. For $\sigma = 1.0$ Å, the fine structural features of the water electron density profile clearly evolve with time reflecting (re-) distribution of water inside the enzyme and/or relatively small conformational changes of the enzyme. It cannot be distinguished how water equilibration and conformational fluctuations individually affects the fine structure of $\rho_c(z)$, but the dependence on these parameters demonstrates why $\rho_c(z)$ cannot straightforwardly be calculated from a static x-ray structure.

To further illustrate the information that is provided by $\rho_c(z)$, Fig. 6 displays $\rho_c^{open}(z)$ and $\rho_c^{closed}(z)$ in selected orientations relative to n_z. Despite a 3-Å smearing, fine structure persists in all representations and the two conforma-

tions in the same orientation lead unambiguously to different profiles. Hence, we conclude that $\rho_c(z)$ can be used for unique characterization of the orientation and conformation of the enzyme.

Experimental and calculated electron densities

We investigated both the wt Tll and the S146A mutant adsorbed at the air-water interface by x-ray reflectivity (Fig. 7 *a*). The corresponding electron density profiles, $\rho_e^{wt}(z)$ and $\rho_e^{S146A}(z)$ obtained through Eq. 2 are shown in Fig. 7 *b* and both profiles show distinct features. The fine structure featured in $\rho_e(z)$ is independent of the methods used to invert the data (compare Eq. 2), and no modulations occur in the profile of pure water using any of these methods. Hence, $\rho_e^{wt}(z)$ and $\rho_e^{S146A}(z)$ provide distinct molecular fingerprints of the two enzymes at the interface. The different fine structures featured in $\rho_e^{wt}(z)$ and $\rho_e^{S146A}(z)$ suggest that the spatial resolution of $\rho_e(z)$ could be sufficient to differentiate experimentally between conformations and/or orientations of Tll at the interface. X-ray diffraction from S146A adsorbed at an air-water interface was measured using a liquid surface diffractometer (Kjaer, 1994; Jensen et al., 2001b). For wt Tll no diffraction was observed. The diffraction data of S146A correspond either to a hexagonal or to a rectangular unit cell (Kjaer, 1994) with areas of 2400 Å^2 or 1200 Å^2 per Tll, respectively (further details will be published elsewhere).

The x-ray reflectivity data inversion in Eq. 2 is hampered by the crystallographic phase problem and multiple $\rho_e^{wt}(z)$ and $\rho_e^{S146A}(z)$ resulted from the respective reflectivity curves. By comparison of the experimental electron density profiles $\rho_e^{wt}(z)$ and $\rho_e^{S146A}(z)$ with $\rho_c^{open}(z)$ and $\rho_c^{closed}(z)$, as done in Fig. 6, the profiles that were not physically meaningful were easily discarded. Recall that $\rho_e^{wt}(z)$ and $\rho_e^{S146A}(z)$ result from lateral averages over an area of 2 × 50 mm^2 corresponding to contributions from ~10^{13} enzymes. In this respect, $\rho_e(z)$ is determined fundamentally different from $\rho_c(z)$, which is calculated as an average over a number of enzyme conformations that is several orders of magnitude smaller than 10^{13}.

As discussed earlier, comparison between $\rho_e(z)$ and $\rho_c(z)$ is only appropriate for $\sigma = 3.0$ Å (Braslau et al., 1985). For $\sigma = 1.0$ Å, $\rho_c^{closed}(z)$ and $\rho_c^{open}(z)$ obtained for the two conformations of Tll in the same orientation are clearly different (Fig. 6) and display more fine structure than $\rho_e^{wt}(z)$ and $\rho_e^{S146A}(z)$. The superposition of the two conformations presented in Fig. 1 indicates that the structural differences between the two conformations mainly amount to the lid region. In contrast, $\rho_c(z)$ indicates that there are differences in the whole protein due to the different conformations sampled during the simulations. Even for $\sigma = 3.0$ Å, fine structural features persist suggesting that molecular information of the adsorbed enzyme can be deduced from fitting $\rho_c(z)$ ($\sigma = 3.0$ Å) to $\rho_e(z)$. According to Fig. 7, structural
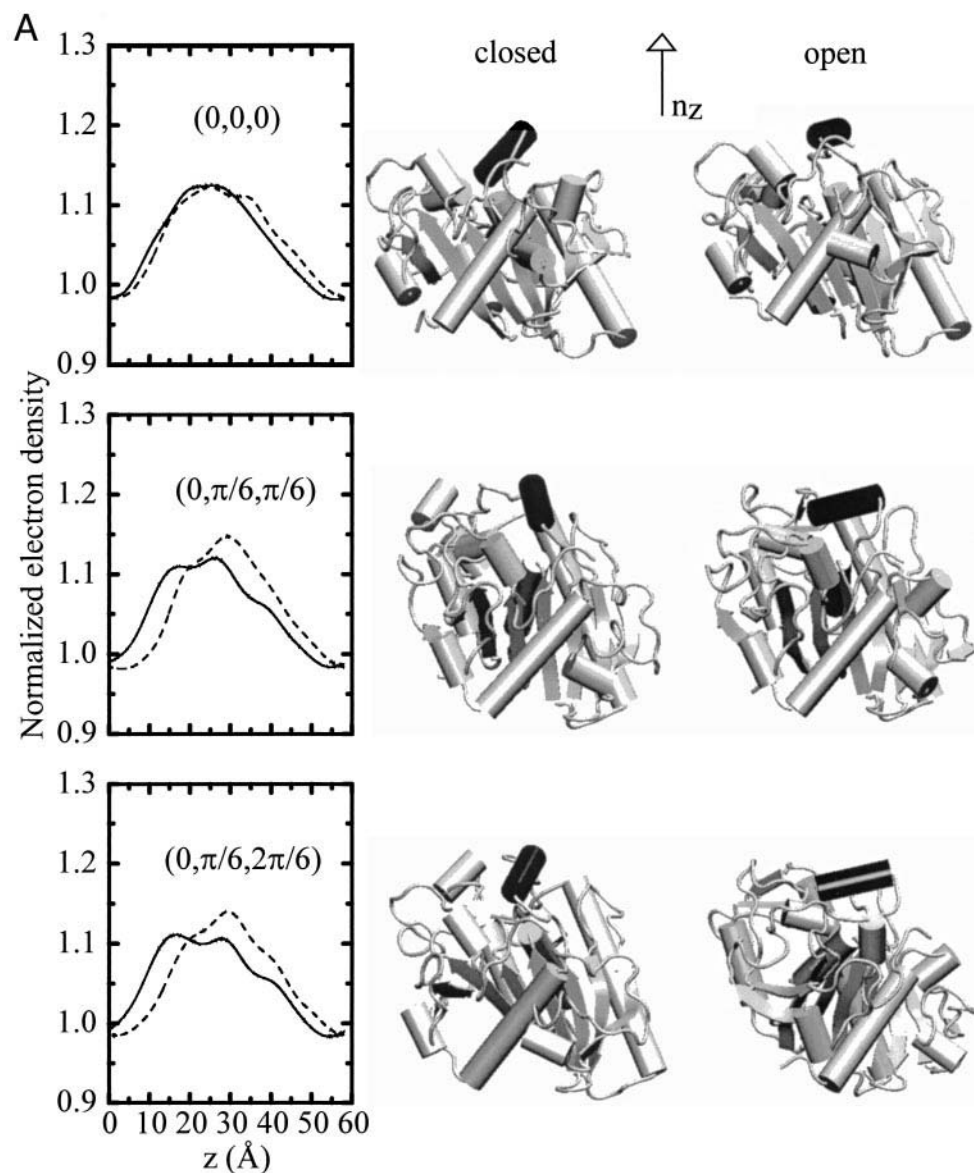
FIGURE 6 Orientation specific electron density profiles for selected orientations of the closed (*solid lines*) and open (*dashed lines*) conformation of Tll are shown in *A* to *C*. Values for (ϕ', θ', ψ') given in all panels indicate the enzyme orientation relative to n_z (Fig. 1). Only (θ', ψ') vary (see text for details), because $\rho_c(z)$ is invariant to rotations around the z axis (i.e., to the ϕ'-value). Snapshots of Tll taken after 2 ns of simulation of the open and closed conformation are shown in orientations referring to the particular electron density profile. The active site lid residues are displayed as a black tube.

information over an interval of $\sim$25 Å can be taken into account when fitting the profiles.

Quantitative comparison

To quantify the comparison of $\rho_c(z)$ with $\rho_e(z)$ we carried out least squares fits of $\rho_c(z)$ to both $\rho_e^{wt}(z)$ and to $\rho_e^{S146A}(z)$ using Eqs. 5 and 6. Although we did not carry out simulations on S146A we know from our earlier simulations of S146A (Peters et al., 1998) that structural differences between S146A and wt Tll are restricted to a few local regions in the protein. We therefore consider $\rho_c^{wt}(z)$ as a reasonable approximation for

$\rho_c^{S146A}(z)$. There is experimental evidences that wt Tll and S146A bind differently to hydrophobic-hydrophilic interfaces (Peters et al., 1998), which is in accord with the characteristic differences featured by $\rho_e^{wt}(z)$ and $\rho_e^{S146A}(z)$ in Fig. 7.

The three best fitting orientations for the applied value of $\rho_e^{H_2O}$ ($= 0.325$ Å^{-3}) and the parameter f are compiled in Table 1 [fit of $\rho_c(z)$ to $\rho_e^{wt}(z)$] and Table 2 [fit of $\rho_c(z)$ to $\rho_e^{S146A}(z)$]. The corresponding electron density profiles are displayed in Figs. 8 and 9 together with snapshots of the two best fitting enzyme orientations of each conformation. To further quantify the quality of the fits, we calculated the resulting variances between $\rho_c(z)$ and $\rho_e(z)$ denoted σ_{e-c} on the fitted interval.
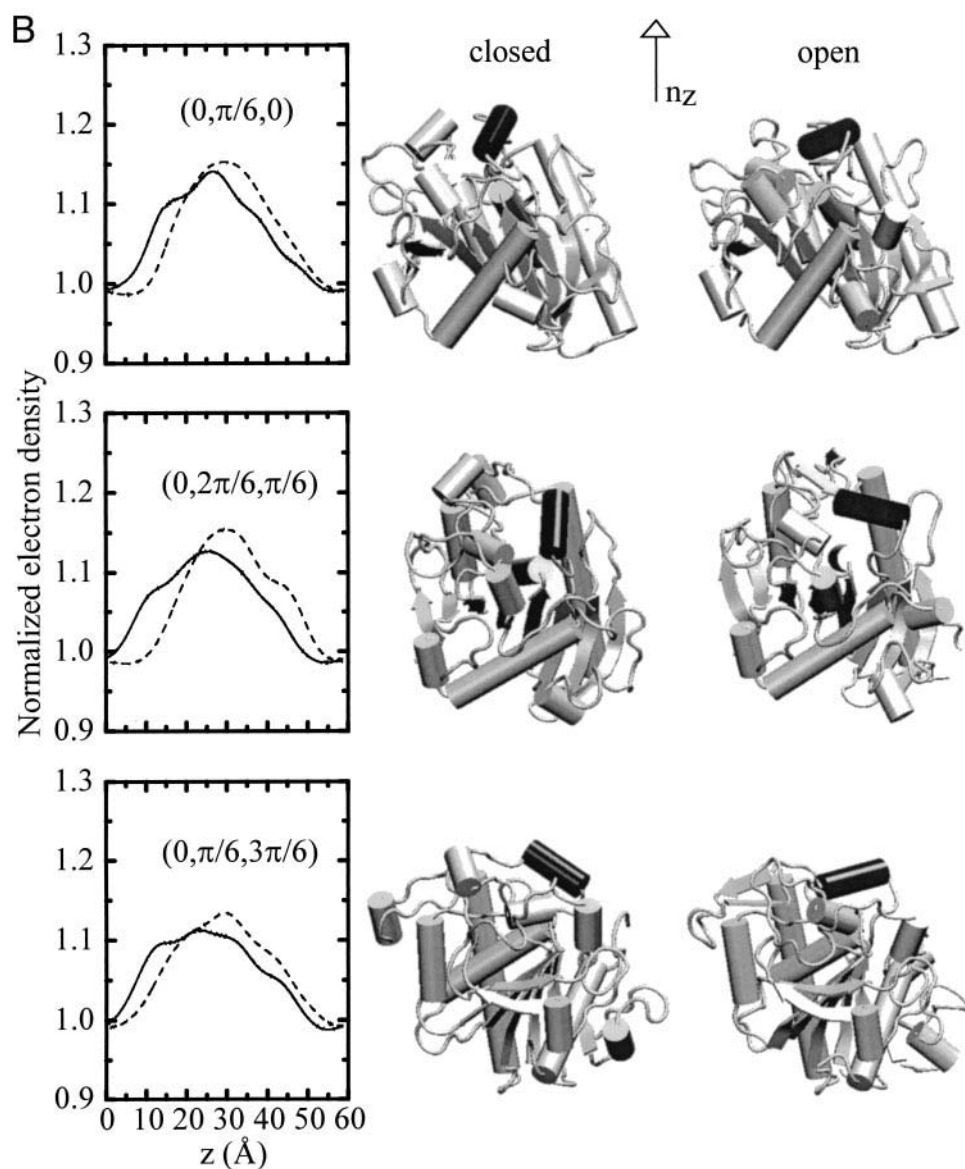
Fig. 6. Continued.

To deduce the experimental area, A_e, we used the time averaged simulation box area, A_c, (perpendicular to n_z), which is 3387 Å^2 ($\simeq$3400 Å^2) and 3469 Å^2 ($\simeq$3450 Å^2) for the simulation box containing the closed and open conformation of Tll, respectively. Because $V_c/V_e \sim A_c/A_e$ using $L_{z,c} = L_{z,e} \simeq 59$ Å we have $A_e = A_c/f$. We solved iteratively for A_e by varying f using the above values for A_c. This leads to the different areas per molecule listed in Tables 1 and 2 and in Figs. 8 and 9. For instance an f value above 1.0 implies that A_e is smaller than A_c.

For the fit of $\rho_c(z)$ to $\rho_e^{wt}(z)$ we find, according to the variances σ_{e-c} in Table 1, that the orientation $(0, 4\pi/6, \pi/6)$ of the open conformation fits $\rho_e^{wt}(z)$ best. The corresponding value for A_e is $\simeq$2300 Å^2. For the closed conformation the orientation, which furnishes the best fit to $\rho_e^{wt}(z)$ is $(0, \pi/6,$

$2\pi/6)$ with $A_e \simeq$1900 Å^2. However, σ_{e-c} is significantly larger and identical to the value for the second best fitting orientation of the open conformation $(0, 4\pi/6, 9\pi/6)$ with $A_e \simeq$2300 Å^2. For the fit of $\rho_c(z)$ to $\rho_e^{S146A}(z)$ we find significantly lower variances (Table 2) for several orientations with areas between $\simeq$2300 Å^2 and $\simeq$2800 Å^2. The best fitting orientation is $(0, 4\pi/6, 9\pi/6)$ with $A_e \simeq$2300 Å^2. All deduced areas conform best to the diffraction result obtained for S146A of 2400 Å^2 per molecule (hexagonal unit cell), whereas $A_e \simeq$1200 Å^2 (rectangular unit cell) seems unlikely. Simple calculations based on the enzyme dimension also support an area of 2400 Å^2. A neutron diffraction study of wt Tll at a surfactant-water interface deduced the volume fraction of interfacially bound enzyme. However, this could not be translated into an area per
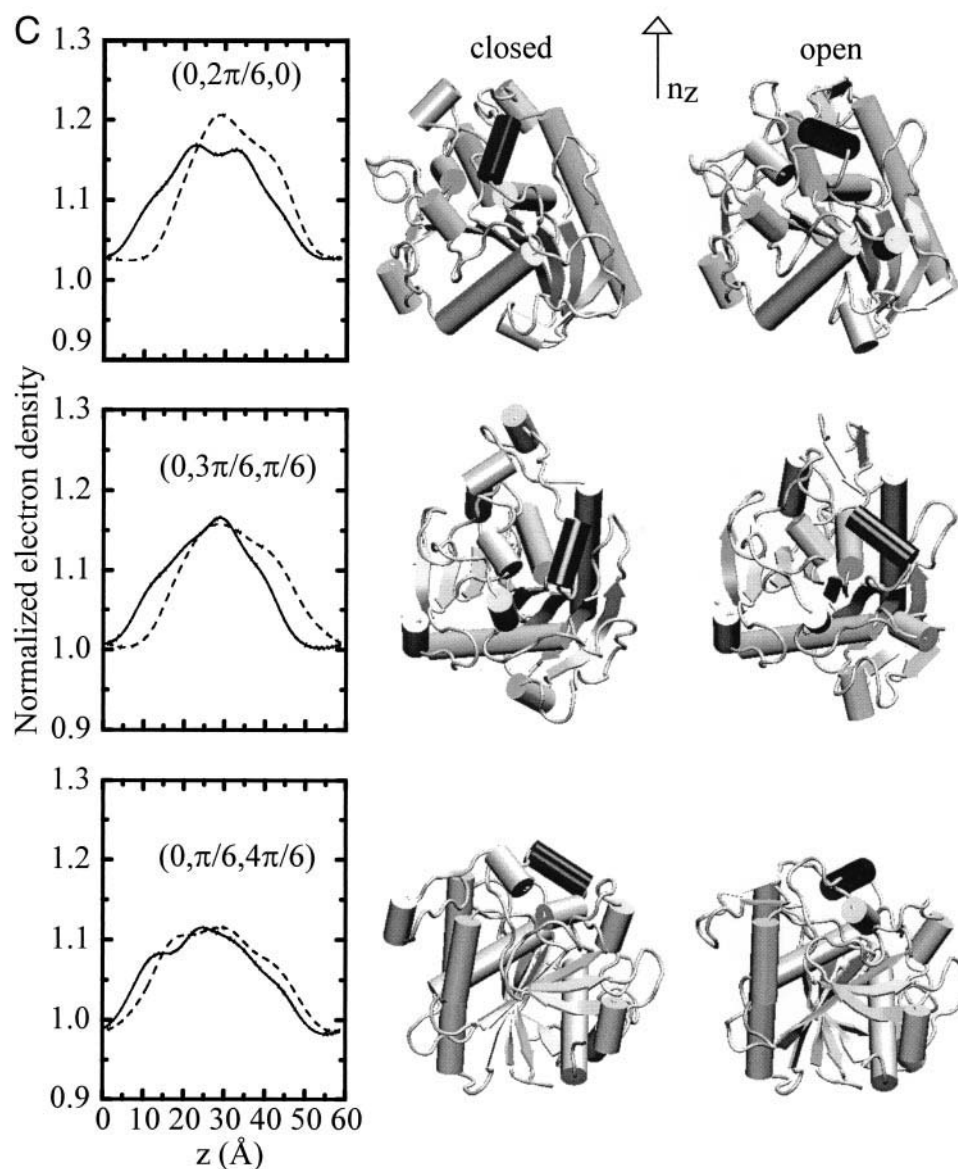
Fig. 6. Continued.

molecule (Lee et al., 1999). In the fit of $\rho_c(z)$ to $\rho_e^{wt}(z)$ and of $\rho_c(z)$ to $\rho_e^{S146A}(z)$ the end point of the region fitted is $z \simeq 40$ Å, which agrees well with the normal dimension of Tll ($\simeq 45$ Å). The 40-Å region therefore captures the relevant normal dimension of the enzyme and confirms the presence of an adsorbed monolayer of both wt Tll and S146A in the two experiments.

For the best fitting wt Tll orientation [$\rho_c^{open}(z)$ to $\rho_e^{wt}(z)$], the lid is positioned ~120 degrees away from n_z (see also Fig. 1). According to σ_{e-c}, the fit of $\rho_c^{open}(z)$ to $\rho_e^{wt}(z)$ was better than the fit of $\rho_c^{closed}(z)$ to $\rho_e^{wt}(z)$. For S146A, the orientations $(0, \pi/6, 6\pi/6)$, $(0, \pi/6, 7\pi/6)$, $(0, \pi/6, 5\pi/6)$, and $(0, 4\pi/6, 2\pi/6)$ [fit of $\rho_c^{open}(z)$ to $\rho_e^{S146A}(z)$] and $(0, \pi/6, 4\pi/6)$, $(0, 3\pi/6, 10\pi/6)$, and $(0, 2\pi/6, 3\pi/6)$ [fit of $\rho_c^{closed}(z)$

to $\rho_e^{S146A}(z)$] cannot be discerned statistically considering the respective values of σ_{e-c} and the standard deviation of $\rho_c(z)$ (Fig. 9). As indicated by the results in Tables 1 and 2, several orientations therefore fit the experimental profiles equally good. The general trend is that the open conformation, which in fact should be characterized as a partially open conformation (discussed in the next section), provides the best fits to both $\rho_e^{wt}(z)$ and $\rho_e^{S146A}(z)$.

Partially open Tll conformation

A dynamic equilibrium between a so-called preactivated, yet closed, and a closed, activated (but catalytically inactive) conformation of Tll was reported by crystallographic trapping of
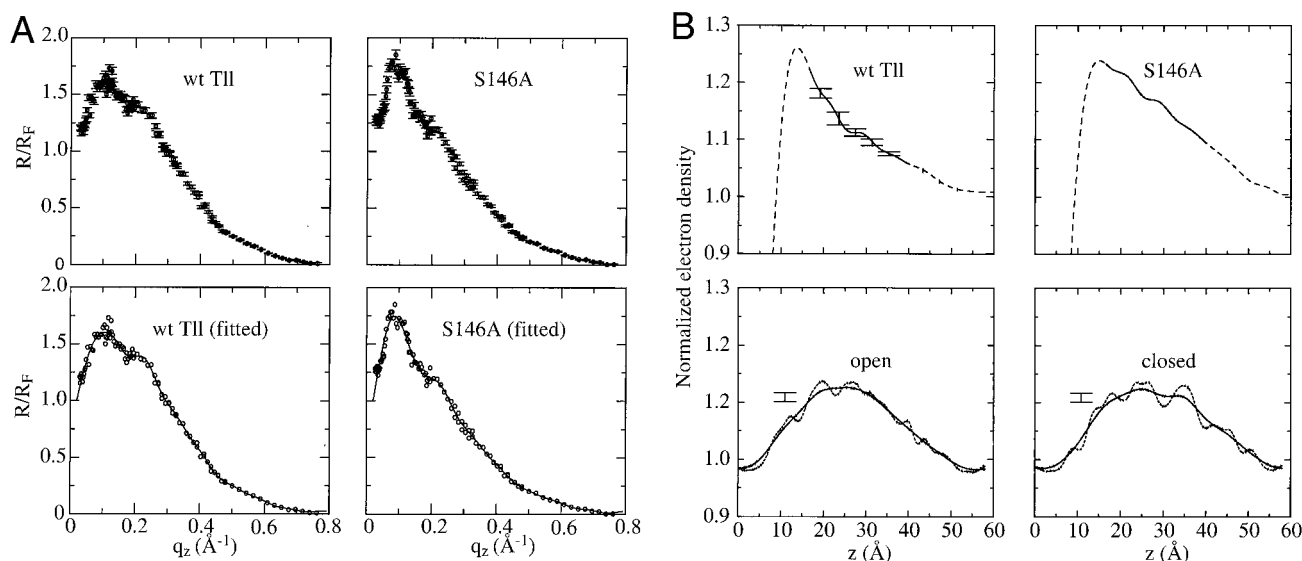
FIGURE 7 (A) Measured reflectivity curves with standard deviations for wt Tll and S146A (*upper panels*) and least squares fits to the measured curves (*lower panels*; measured curves included for comparison). The background was determined experimentally by offsetting the detector from the specular position (out of the scattering plane). The normalization was determined experimentally by measuring the direct beam intensity. Thus, neither background nor normalization introduces any adjustable parameters. The inversion of $R(q_z)/R_F(q_z)$ was performed by a model-independent method, writing $\rho_e(z)$ as a weighted sum of cubic-spline functions (Pedersen, 1992; Pedersen and Hamley, 1994; Hamley and Pedersen, 1994). The reflectivity is then calculated for such a model. Least-squares fitting to the measured data, with a smoothness constraint on the model for stabilization, results in the final $\rho_e(z)$ (Pedersen and Hamley, 1994). Due to the so-called phase problem of x-ray scattering the data inversion is not in general unique. As seen from Fig. *a* the Fourier cutoff is approximately $q_z \simeq 0.85 \, \text{Å}^{-1}$. (B) Experimental electron density profiles for wt Tll and S146A (*upper panels*) and calculated electron density profiles for wt Tll in open and closed conformation in the (0, 0, 0) orientation (*lower panels*). All profiles are normalized with the electron density of bulk water. In the upper panels, the solid region indicates the part of the electron density that is used in comparison with the calculated profiles. The standard deviation within this region is included for the wt Tll profile (similar values apply to the S146A profile). The calculated profiles in the lower panels, averaged over 3 ns, are for $\sigma = 1.0 \, \text{Å}$ (*dotted lines*) and for $\sigma = 3.0 \, \text{Å}$ (*solid lines*). Average standard deviations (along *z*) are shown next to the profiles.

TABLE 1 **Quantitative comparison of calculated and experimental electron density profiles of wt Tll extracted from X-ray reflectivity data [fit of $\rho_c(z)$ to $\rho_{wt}^e(z)$]**

f	A_e (Å)	Closed-1	σ_{e-c}	Closed-2	σ_{e-c}	Closed-3	σ_{e-c}
1.0	~3400	$(0, 2\pi/6, 6\pi/6)$	0.00523	$(0, 4\pi/6, 3\pi/6)$	0.00704	$(0, 3\pi/6, 2\pi/6)$	0.00710
1.1	~3150	$(0, \pi/6, 11\pi/6)$	0.00404	$(0, \pi/6, 10\pi/6)$	0.00521	$(0, 2\pi/6, 0)$	0.00560
1.2	~2800	$(0, \pi/6, 11\pi/6)$	0.00400	$(0, 0, 0)$	0.00436	$(0, \pi/6, 10\pi/6)$	0.00488
1.3	~2600	$(0, \pi/6, 11\pi/6)$	0.00414	$(0, \pi/6, 0)$	0.00430	$(0, 0, 0)$	0.00458
1.4	~2400	$(0, \pi/6, 11\pi/6)$	0.00416	$(0, \pi/6, 0)$	0.00417	$(0, 0, 0)$	0.00439
1.5	~2250	$(0, \pi/6, 11\pi/6)$	0.00361	$(0, 0, 0)$	0.00382	$(0, \pi/6, 0)$	0.00397
1.6	~2100	$(0, 0, 0)$	0.00331	$(0, \pi/6, 0)$	0.00345	$(0, \pi/6, \pi/6)$	0.00362
1.7	~2000	$(0, 0, 0)$	0.00287	$(0, \pi/6, 0)$	0.00298	$(0, \pi/6, \pi/6)$	0.00314
1.8	~1900	$(0, \pi/6, 2\pi/6)$	0.00110	$(0, \pi/6, 0)$	0.00258	$(0, \pi/6, \pi/6)$	0.00272
1.9	~1800	$(0, \pi/6, 2\pi/6)$	0.00194	$(0, \pi/6, 0)$	0.00223	$(0, \pi/6, \pi/6)$	0.00236
f	A_e (Å)	open-1	σ_{e-c}	open-2	σ_{e-c}	open-3	σ_{e-c}
1.0	~3450	$(0, 4\pi/6, 8\pi/6)$	0.00438	$(0, 2\pi/6, 7\pi/6)$	0.00550	$(0, 4\pi/6, 5\pi/6)$	0.00724
1.1	~3150	$(0, \pi/6, \pi/6)$	0.00336	$(0, 4\pi/6, 8\pi/6)$	0.00469	$(0, 2\pi/6, 7\pi/6)$	0.00518
1.2	~2900	$(0, 0, 0)$	0.00253	$(0, \pi/6, \pi/6)$	0.00265	$(0, 4\pi/6, 8\pi/6)$	0.00398
1.3	~2650	$(0, \pi/6, \pi/6)$	0.00205	$(0, \pi/6, 2\pi/6)$	0.00217	$(0, 0, 0)$	0.00245
1.4	~2500	$(0, \pi/6, \pi/6)$	0.00157	$(0, \pi/6, 2\pi/6)$	0.00167	$(0, 0, 0)$	0.00190
1.5	~2300	$(0, 4\pi/6, \pi/6)$	0.00030	$(0, 4\pi/6, 9\pi/6)$	0.00109	$(0, 0, 0)$	0.00146

The area per adsorbed wt Tll (A_e) was deduced from the quantity $A_e = A_c/f$. The value used for $\rho_e^{H_2O}$ was 0.325 Å^{-3} (see Eqs. 5, 6, and text). The three profiles of the closed and open conformations of wt Tll, respectively, that are fitting the experimental data the best, second best, and third best are denoted closed-1, closed-2, closed-3, and open-1, open-2, open-3, respectively. The corresponding variances σ_{e-c} were calculated between 740 experimental (*e*) and calculated (*c*) data points separated by the slab width $dz = 0.03$ Å on the fitted interval (see also Figs. 6 and 8).

TABLE 2 Quantitative comparison of calculated wt Tll electron density profiles with the experimental S146A electron density profile extracted from x-ray reflectivity data (fit of $\rho_c(z)$ to $\rho_e^{S146A}(z)$, see caption to Table 1 for more details)

f	$A_e(Å)$	closed-1	σ_{e-c}	closed-2	σ_{e-c}	closed-3	σ_{e-c}
1.0	~3400	$(0, \pi/6, 0)$	0.00333	$(0, 4\pi/6, 11\pi/6)$	0.00588	$(0, \pi/6, 4\pi/6)$	0.00863
1.1	~3150	$(0, \pi/6, \pi/6)$	0.00360	$(0, \pi/6, 3\pi/6)$	0.00560	$(0, \pi/6, 3\pi/6)$	0.00676
1.2	~2800	$(0, 3\pi/6, 10\pi/6)$	0.00056	$(0, \pi/6, 3\pi/6)$	0.00368	$(0, \pi/6, 3\pi/6)$	0.00045
1.3	~2600	$(0, 3\pi/6, 10\pi/6)$	0.00010	$(0, \pi/6, 2\pi/6)$	0.00232	$(0, \pi/6, 3\pi/6)$	0.00270
1.4	~2400	$(0, 3\pi/6, 10\pi/6)$	0.00011	$(0, \pi/6, 2\pi/6)$	0.00128	$(0, \pi/6, 3\pi/6)$	0.00134
1.5	~2250	$(0, \pi/6, 4\pi/6)$	0.00008	$(0, 2\pi/6, 3\pi/6)$	0.00019	$(0, 3\pi/6, 10\pi/6)$	0.00057
f	$A_e(Å)$	open-1	σ_{e-c}	open-2	σ_{e-c}	open-3	σ_{e-c}
1.0	~3450	$(0, 0, 0)$	0.00656	$(0, 4\pi/6, \pi/6)$	0.00712	$(0, 4\pi/6, 2\pi/6)$	0.00835
1.1	~3150	$(0, \pi/6, 3\pi/6)$	0.00213	$(0, 4\pi/6, 2\pi/6)$	0.00238	$(0, 4\pi/6, \pi/6)$	0.00370
1.2	~2900	$(0, 4\pi/6, 2\pi/6)$	0.00111	$(0, 4\pi/6, 9\pi/6)$	0.00136	$(0, 4\pi/6, \pi/6)$	0.00199
1.3	~2650	$(0, 4\pi/6, 2\pi/6)$	0.00018	$(0, 4\pi/6, 9\pi/6)$	0.00033	$(0, 4\pi/6, \pi/6)$	0.00063
1.4	~2500	$(0, 4\pi/6, 9\pi/6)$	0.00005	$(0, \pi/6, 4\pi/6)$	0.00028	$(0, \pi/6, 6\pi/6)$	0.00045
1.5	~2300	$(0, \pi/6, 6\pi/6)$	0.00008	$(0, \pi/6, 7\pi/6)$	0.00009	$(0, \pi/6, 5\pi/6)$	0.00013

these conformations (Brzozowski et al., 2000). The closed activated conformation should not be confused with the catalytic active, open conformation in the present study; the closed activated state is identical to our closed conformation (Brzozowski et al., 2000). These crystal structures suggest that the interfacial activation of Tll might well be a multistep process

involving more than two conformational transitions before a fully active conformation is assumed.

One could speculate whether there exists a dynamic equilibrium between open and closed conformations at the interface, or the enzyme is adsorbed in a partially open/ partially closed conformation. The presence of a dynamical
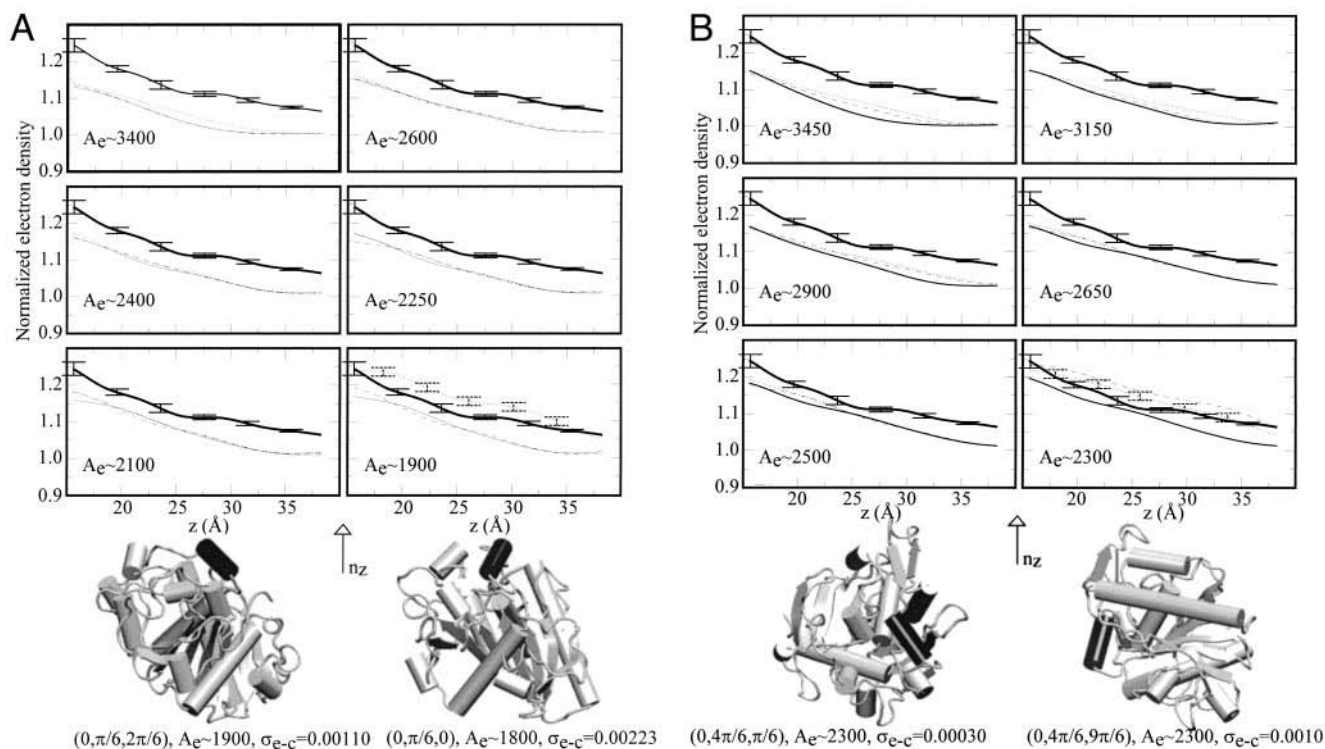

FIGURE 8   Three best fitting orientation specific profiles resulting from a fit of the calculated electron density profile to the experimental electron density profile for wt Tll; (*A*) closed conformation and (*B*) open conformation. Only the fitted parts of the best (*dotted lines*), second best (*dashed lines*), and third best (*thin solid lines*) are shown together with the fitted part of the experimental profile (*bold solid lines*). The deduced area per lipase molecule (in Å²) appears in each panel. See caption to Table 1 and text for more details. A snapshot taken after 2 ns of simulation of Tll in the two best fitting, different orientations according to Table 1 appears below the electron density profiles. The active site lid residues are displayed as a black tube. Standard deviations for experimental and calculated data are indicated by solid and dashed error bars, respectively.
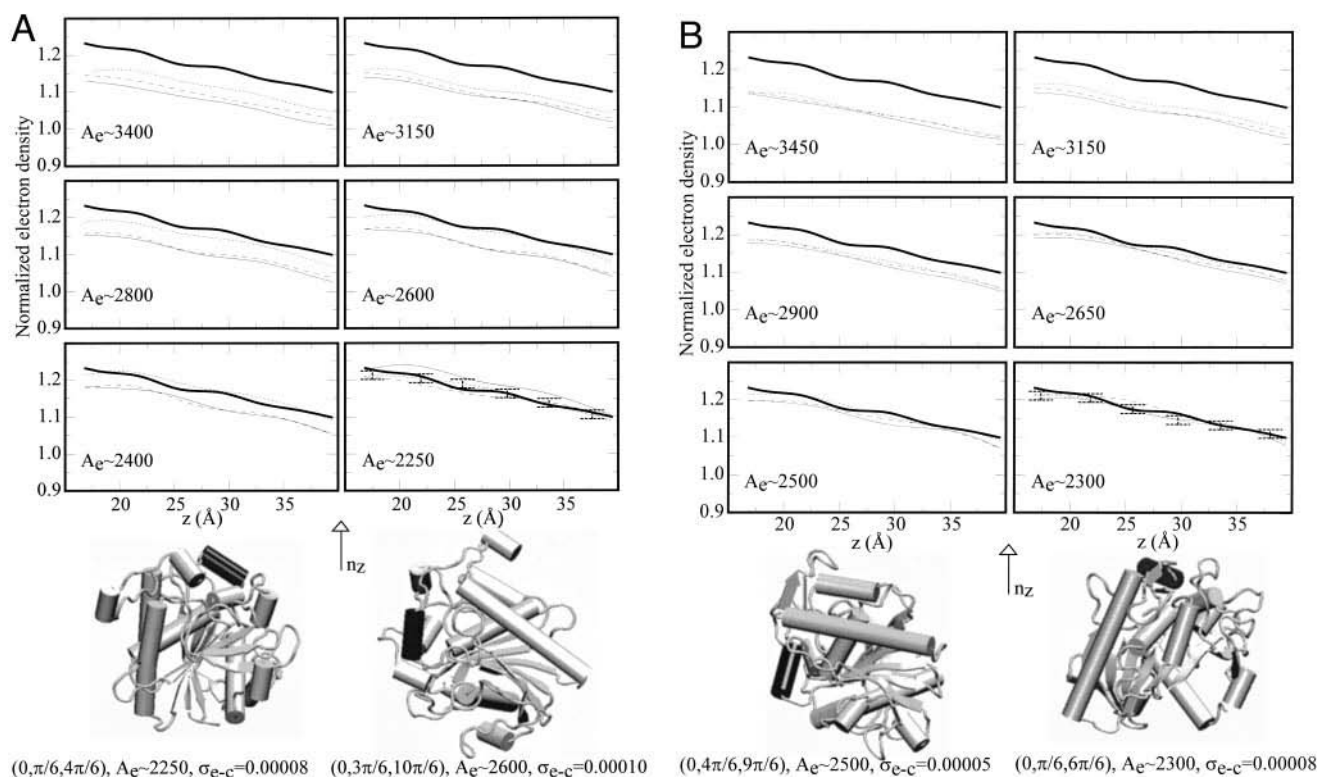
FIGURE 9   Three best fitting orientation specific profiles resulting from a fit of the calculated electron density profile to the experimental electron density profile for S146A; (*A*) closed conformation and (*B*) open conformation. See caption to Fig. 8 for more details. Dashed error bars indicate standard deviations of the calculated data.

equilibrium between the closed activated (our closed) and fully activated (our open) conformation remains to be confirmed experimentally. The simulations of Tll (open) showed that lid closed partially resulting in the conformation shown in Fig. 1. Focusing on the lid residues 84 to 95, the RMSD between the C_α atoms of these residues along the trajectory relative to the initial open (crystal) structure are found to be 3.5 Å (2 ns), 4.4 Å (4 ns), 3.9 Å (6 ns), 3.8 Å (8 ns), and 4.1 Å (10 ns). Accordingly, the lid does not close completely. The intermediate conformation should be characterized as slightly more open than closed, because the RMSD values of the C_α atoms of the same lid residues relative to the initial closed (crystal) structure are 5.5 Å (2 ns), 5.3 Å (4 ns), 5.4 Å (6 ns), 5.4 Å (8 ns), and 5.7 Å (10 ns). These RMSD values indicate that the observed lid closure is a significant conformational change that most likely occurs due to a shielding of the hydrophobic part of the lid from the aqueous solvent. The lid of the closed conformation remained essentially in the same conformation over the 12-ns simulation time.

CONCLUSION

Biomolecules can assemble at the air-water interface and form two-dimensional crystalline layers (Rapaport et al.,

2000; Alonso et al., 2001). As demonstrated here protein layers can be investigated by using x-ray techniques. Specifically, we have investigated electron density profiles of wt Tll and a mutant of Tll in the case where these enzymes adsorb at the air-water interface. The interpretation of the resulting electron density profiles in terms of conformation and orientation of the enzyme relies on the amount of fine structure present as shown by the computation of the electron density profiles for the active and inactive conformation of wt Tll. Although the interpretation of such experiments on a molecular level in nontrivial, the experimental electron densities were interpreted using the corresponding profiles computed from MD trajectories. The analysis was accomplished by developing a computational scheme that allowed for extraction of several electron density profiles from a single trajectory, and by subsequently bringing these on the same scale as the experimental profiles. Convergence of the computed profiles and reduction of statistical noise were ensured by performing simulations for several ns. Our computational results indicate that there is in principle sufficient information in the electron density profiles to uniquely characterize the orientation and conformation of the adsorbed enzyme and even to differentiate between closely related enzymes. In fact, we performed similar calculations on the open and closed conformations of *Rhizo-*

mucor meihei lipase and found that the resulting electron density profiles are different from those of Tll. The comparison of the calculated and measured profiles is predominantly limited by the intrinsic surface roughness in the experiment. We find that the experiment can hardly distinguish between open and closed conformation of Tll. A least squares fit of the calculated profiles to the experimental profile yields an area per adsorbed molecule between 2300 and 2800 Å for both wt and the mutant, which is in accordance with our x-ray diffraction result, thereby confirming the existence of an adsorbed monolayer. The best fitting orientation of wt Tll has the lid oriented at an angle of ∼120 degrees away from the surface normal. The orientation of S146A has the lid oriented 30 to 120 degrees away from the surface normal. The simulations furthermore suggest that the conformation of the adsorbed enzyme might be in a partially open conformation.

REFERENCES

Alonso, C., I. Kuzmenko, T. R. Jensen, K. Kjaer, M. Lahav, and L. Leiserowitz. 2001. Selfassembly of crystalline films of interdigitated long-chain cholesteryl esters at the air-water interface. *J. Phys. Chem. B.* 105:8563–8568.

Als-Nielsen, J., D. Jacquemain, K. Kjaer, F. Leveiller, M. Lahav, and L. L. 1994. Principles and applications of grazing incidence x-ray and neutron scattering from ordered monolayers at the air-water interface. *Phys. Rep.* 246:251–313.

Als-Nielsen, J., and D. McMorrow. 2001. Elements of Modern X-Ray Physics. Wiley, New York.

Ball, A., R. Nielsen, M. H. Gelb, and B. H. Robinson. 1999. Interfacial membrane docking of cytosolic phospholipase a2, o2 domain using electrostatic potential-modulated spin relaxation magnetic resonance. *Proc. Natl. Acad. Sci. U.S.A.* 96:6637–6642.

Berendsen, H., R. van der Spoel, and D. van Drunen. 1995. Gromacs: a message-passing parallel molecular dynamics implementation. *Comp. Phys. Commun.* 91:43–56.

Berendsen, H. J. C., J. P. M. Postma, W. F. van Gunsteren, A. DiNola, and J. R. Haak. 1984. Molecular dynamics with coupling to an external bath. *J. Chem. Phys.* 81:3684–3689.

Bernstein, F. C., T. F. Koetzle, G. J. B. Williams, E. F. Meyer, J. R. Brice, M. D. Rogers, O. Kennard, T. Shimanouchi, and M. Tasumi. 1977. The protein data bank: a computer based archival file for macromolecular structures. *J. Mol. Biol.* 112:535–542.

Born, M., and E. Wolf. 1984. Principles of Optics. Pergamon Press, Oxford, UK.

Brady, L., A. M. Brzozowski, Z. S. Derewenda, E. Dodson, S. Tolley, J. P. Turkenburg, L. Christiansen, B. Huge-Jensen, L. Norskov, L. Thim, and U. Menge. 1990. A serine protease forms the catalytic center of a triacylglycerol lipase. *Nature.* 343:767–770.

Braslau, A., M. Deutsch, P. S. Pershan, A. H. Weiss, J. Als-Nielsen, and J. Bohr. 1985. Surface roughness of water measured by x-ray reflectivity. *Phys. Rev. Lett.* 54:114–117.

Brzozowski, A. M., U. Derewenda, Z. S. Derewenda, G. G. Dodson, D. M. Lawson, J. P. Turkenburg, F. Bjorkling, B. Huge-Jensen, S. A. Patkar, and L. Thim. 1991. A model for interfacial activation in lipases from the structure of fungal lipase-inhibitor complex. *Nature.* 351:491–494.

Brzozowski, A. M., Z. S. Derewenda, E. J. Dodson, G. G. Dodson, and J. P. Turkenburg. 1992. Structure and molecular-model refinement of rhizomucor-miehei triacylglyceride lipase-a case-study of the use of simulated annealing in partial model refinement. *Acta Crystall. B.* 48: 307–319.

Brzozowski, A. M., H. Savage, C. S. Verma, J. P. Turkenburg, D. M. Lawson, A. Svendsen, and S. A. Patkar. 2000. Structural origins of the interfacial activation in *Thermomyces (Humicola) lanuginosa* lipase. *Biochemistry.* 39:15071–15082.

Cajal, Y., A. Svendsen, V. Girona, S. A. Patkar, and M. A. Alsina. 2000. Interfacial control of lid opening in *Thermomyces lanuginosa* lipase. *Biochemistry.* 39:413–423.

Derewenda, U., A. M. Brzozowski, D. M. Lawson, and Z. S. Derewenda. 1992. Catalysis at the interface: the anatomy of a conformational change in a triglyceride lipase. *Biochemistry.* 31:1532–1541.

Derewenda, U., L. Swenson, Y. Wei, R. Green, P. M. Kobos, R. Joerger, M. J. Haas, and Z. S. Derewenda. 1994. Conformational lability of lipases observed in the absence of an oil-water interface: crystallographic studies of enzymes from the fungi *Humicola lanuginosa* and *Rhizopus delemar. J. Lipid Res.* 35:524–534.

Grochuiski, P., L. Yunge, J. Schrag, F. Bouthillier, P. Smith, D. Harrison, B. Rubin, and M. Cygler. 1993. Insights into interfacial activation from an open structure of *Candida rugosa* lipase. *J. Biol. Chem.* 268: 12843–12847.

Hamley, I. W., and J. S. Pedersen. 1994. Analysis of neutron and x-ray reflectivity data in theory. *J. Appl. Crystallog.* 27:29–35.

Jensen, T. R., and K. Kjaer 2001. Structural properties and interactions of thin films at the air-liquid interface explored by synchrotron x-ray scattering. *In* Novel Methods to Study Interfacial Layers, Studies in Interface Science, Volume II. D. Mobius and R. Miller, editors. Elsevier Science, B. V. 205–254.

Jensen, T. R., K. Kjaer, K. Balashev, and T. Bjørnholm. 2001. Novel methods for studying lipids and lipases and their mutual interaction at interfaces: Part II. Surface sensitive synchrotron x-ray scattering. *Biochemie.* 83:399–408.

Jutila, A., K. Zhu, S. A. Patkar, J. Vind, A. Svendsen, and P. K. J. Kinnunen. 2000. Detergent-induced conformational changes of *Humicola lanuginosa* lipase studied by fluorescence spectroscopy. *Biophys. J.* 78:1634–1642.

Kinnunen, P., A. Kõiv, and P. Mustonen. 1993. Pyrene-Labelled Lipids as Fluorescent Probes in Studies on Biomembranes and Membrane Models. *In* Fluorescence Spectroscopy. O. Wolfbeis, editor. Springer Verlag, New York. 159–171.

Kjaer, K. 1994. Some simple ideas on X-ray reflection and grazing-incidence diffraction from thin surfactants films. *Phys. B.* 198:100–109.

Lee, L.-T., B. K. Jha, M. Malmsten, and K. Holmberg. 1999. Lipase-surfactant interactions studied by neutron reflectivity and elipsometry. *J. Phys. Chem. B.* 103:7489–7494.

Millar, D. 1996. Fluorescence studies of DNA and RNA structure and dynamics. *Curr. Opin. Struc, Biol.* 6:322–326.

MSI. 1997. QUANTA 97. Molecular Simulations Inc., Burlington, MA.

Panaiotov, M., M. Ivanova, and R. Verger. 1997. Interfacial and temporal organisation of enzymatic lipolysis. *Curr. Opin. Coll. Interf. Sci.* 2:517–525.

Pedersen, J. S. 1992. Model-independent determination of the surface scattering-length-density profile from specular reflectivity data. *J. Appl. Crystallogr.* 25:129–145.

Pedersen, J. S., and I. W. Hamley. 1994. Analysis of neutron and X-ray reflectivity data: II. Constrained least-square methods. *J. Appl. Cryst.* 27:36–49.

Peters, G. H., A. Svendsen, H. Langberg, J. Vind, S. A. Patkar, S. Toxvaerd, and P. K. J. Kinnunen. 1998. Active serine involved in the stabilization of the active site loop in the *Humicola lanuginosa* lipase. *Biochemistry.* 37:12375–12383.

Peters, G. H., S. Toxværd, N. B. Larsen, T. Bjørnholm, K. Schaumburg, and K. Kjaer. 1995. Structure and dynamics of lipid monolayers, implications for enzyme catalysed lipolysis. *Nat. Struct. Biol.* 2:401–409.

Peters, G. H., D. M. F. van Aalten, O. Edholm, S. Toxvaerd, and R. Bywater. 1996a. Dynamics of proteins in different solvent systems: analysis of essential motion in lipases. *Biophys. J.* 71:2245–2251.

Peters, G. H., D. M. F. van Aalten, A. Svendsen, and R. Bywater. 1996b. Essential dynamics of lipase binding sites: the effect of inhibitors of different chain length. *Protein Eng.* 10:149–158.

Ransac, S., Y. Gargouri, H. Moreau, R. Verger, and G. H. de Haas. 1991. Inactivation of pancreatic and gastric lipases by tetrahydrolipstatin and alkyl-dithio-5-(2-nitrobenzoic acid). A kinetic study with 1,2-didecanoyl-*sn*-glycerol monolayers. *Eur. J. Biochem.* 202:395–400.

Ransac, S., G. Rivière, J. M. Soulié, C. Gancet, R. Verger, and G. H. de Haas. 1990. Competitive inhibition of lipolytic enzymes: I. A kinetic model applicable to water-insoluble competitive inhibitors. *Biochim. Biophys. Acta.* 1043:57–66.

Rapaport, H., K. Kjaer, T. R. Jensen, L. Leiserowitz, and D. A. Tirrell. 2000. Crystalline β-sheet monolayers: a new class of ordered molecular templates. *J. Am. Chem. Soc.* 122:12523–12529.

Rubingh, D. N. 1996. The influence of surfactants on enzyme activity. *Curr. Opin. Coll. Interf. Sci.* 1:598–603.

Thuren, T. 1988. A model for the molecular mechanism of interfacial activation of posphoplipase A_2 supporting the substrate theory. *FEBS Lett.* 229:95–99.

van Gunsteren, W. F., and H. J. C. Berendsen. 1987. GROMOS87 Manual. Biomos BV.

van Tilbeurgh, H., M. P. Egloff, C. Martinez, N. Rugani, R. Verger, and C. Cambillau. 1993. Interfacial activation of the lipase procolipase complex by mixed micelles revealed by x-ray crystallography. *Nature.* 362:824.

Verger, R., F. Pattus, G. Piéroni, C. Riviere, F. Ferrato, J. Leonardi, and B. Dargent, 1984. Regulation by the interfacial quality of some biological activities. *Col. Surf.* 10:163–180.

Verger, R., and G. H. de Haas. 1973. Enzyme reactions in a membrane model: 1: A new technique to study enzyme reactions in monolayers. *Chem. Phys. Lipids.* 10:127–136.

Weissbuch, I., R. Popovitz-Biro, M. Lahav, L. Leiserowitz, K. Kjaer, and J. Als-Nielsen. 1997. Molecular self-assembly into crystals at air-liquid interfaces. *In* Advances in Chemical Physics, volume 102. I. Prigogine and S. Rice, editors. John Wiley, New York. 39–120.